JOURNAL OF GUIDANCE, CONTROL, AND DYNAMICS
Vol. 33, No. 1, January–February 2010

Reentry Terminal Guidance Through Sliding Mode Control

Nathan Harl* and S. N. Balakrishnan†
IST-Rolla, Rolla, Missouri 65401

DOI: 10.2514/1.42654

A guidance scheme has been developed for the terminal guidance of an unpowered lifting reentry vehicle during the approach and landing phase. The proposed approach is quite useful for offline trajectory design and allows for trajectories to be generated online through the use of a closed-loop control law. In scenarios in which the reentry vehicle is significantly deviated from its nominal trajectory upon entry into the landing phase, the usefulness of such an online method can be clearly realized. These types of scenarios are of interest for any reentry vehicle, including the space shuttle, since existing guidance approaches during the approach and landing phase involve tracking trajectories created offline. To solve the approach and landing guidance problem, a novel concept called the sliding mode terminal guidance is used in this work. This approach takes advantage of the finite-time-reaching phase of the sliding mode technique to ensure that any desired state constraints can be fulfilled in a finite time. Further, by using a new approach to second-order sliding mode control, analytic solutions are obtained for both the altitude and flight-path angle during the reentry process. The end result of this approach is a closed-loop guidance (control) law, which can be used to generate trajectories that depend only on the initial and final conditions of the approach and landing phase. Simulations shown indicate that the method provides some robustness to variations in the initial downrange and velocity.

Nomenclature

A, B, C	=	nonlinear expressions in guidance law
C_D	=	drag coefficient
C_{D_0}	=	zero-lift drag coefficient
C_L	=	lift coefficient
C_{L_0}	=	zero-angle-of-attack lift coefficient
D	=	drag force, lb
g	=	Earth's gravitational acceleration, 32.174 ft/s^2
H	=	scale height, 8.5 km
h	=	altitude, m
K	=	lift-induced drag coefficient parameter
L	=	lift force, N
m	=	reusable launch vehicle mass, slugs
n	=	control law tuning coefficient
R	=	range to the runway, ft
s	=	sliding surface
S	=	surface area, ft^2
t	=	time, s
V	=	velocity magnitude, ft/s
V_l	=	Lyapunov function
x	=	downrange, ft
α	=	angle of attack, deg
β	=	constant used in control law
γ	=	flight-path angle, deg
ρ	=	air density, slugs/ft^3
ρ_0	=	sea-level air density, 0.0027 slugs/ft^3

Introduction

IN RECENT years, it has become apparent that there is a need for developing advanced reentry guidance technologies that can improve the safety and reliability of reusable launch vehicles (RLVs). In particular, guidance technologies are desired that can accommodate for aerosurface failures, poor vehicle performance, or dispersions from the desired trajectory [1]. These types of technologies are particularly critical during the approach and landing (A&L) reentry phase. Of these sources of uncertainty, this paper focuses on accounting for dispersions from the desired trajectory. However, the method presented in this paper is not intended to compensate for the aerosurface failures.

For the space shuttle [2], the A&L phase is the final phase of the reentry process, beginning at the end of the terminal area energy management phase at an altitude of roughly 10,000 ft and ending with touchdown on the runway. The goal of this flight phase is for the RLV to land at a desired runway with a near-zero vertical velocity. The vertical velocity at touchdown is desired to be below 5 ft/s, but velocities up to 9 ft/s are generally still considered acceptable for the space shuttle [2]. One of the concerns with guidance during the A&L phase is that there is the possibility that crucial control surfaces on the RLV may be damaged during the previous reentry phases, leading to a loss of controllability [1]. Another concern is that upon entering the A&L phase there may be a significant deviation of the RLV from its desired trajectory. This concern is very significant because current space shuttle guidance methods during the A&L phase rely on the shuttle to follow a predetermined trajectory [2]. There is thus a need for A&L guidance technologies that *do not* require predetermined reference trajectories to be implemented, but instead would be capable of obtaining feasible trajectories online.

There have been many previous papers that solve the A&L guidance problem while attempting to minimize the amount of offline information required. Schierman et al. [3–5] presented an approach for obtaining feasible A&L trajectories in the presence of major control surface errors. The authors solved the problem using an optimum-path-to-go (OPTG) approach. In this approach, a large database of neighboring optimal trajectories is first generated *offline*. Then, when integrating the trajectory online, the states are observed at each point and the trajectory is reconfigured to follow the particular offline trajectory that leads to the best performance. Later, Schierman et al. [6,7] used their OPTG approach to account for control surface errors between the atmospheric entry and terminal-area energy-management phases. In [7], the authors also accounted for the scenario of targeting alternative landing locations. Results are presented that show that in the presence of control surface errors, the mission is lost, whereas with the OPTG trajectory reconfiguration approach, the mission is a success.

Bollino et al. [8] proposed a real-time optimal control approach for generating reentry trajectories through a pseudospectral method. The authors used this method to generate online trajectories from the

Presented as Paper 6215 at the 2008 AIAA Atmospheric Flight Mechanics Conference, Honolulu, HI, 18–21 August 2008; received 8 December 2008; revision received 20 August 2009; accepted for publication 22 August 2009. Copyright © 2009 by IST-Rolla, Rolla, MO. Published by the American Institute of Aeronautics and Astronautics, Inc., with permission. Copies of this paper may be made for personal or internal use, on condition that the copier pay the $10.00 per-copy fee to the Copyright Clearance Center, Inc., 222 Rosewood Drive, Danvers, MA 01923; include the code 0731-5090/10 and $10.00 in correspondence with the CCC.

*Engineer, 710 University Drive; nharl@istrolla.com.
†Senior Scientist, 710 University Drive; bala@istrolla.com.

point of atmospheric entry to a flight corridor of approximately 2000 ft altitude. External disturbances due to wind gusts were also incorporated into the analysis. These wind gusts ranged from very small levels to those present in a category 5 hurricane. The authors presented results that show that their method can successfully develop feasible trajectories even in the presence of severe wind gusts. Also, since the authors did not segment the trajectory into phases, their approach is not limited to a specific phase.

Fahroo and Doman [9] developed an approach for trajectory reshaping during approach and landing using a Legendre pseudospectral method. The authors first presented a method for predicting flight envelope constraints and then used this method with the Legendre pseudospectral approach to determine optimal feasible trajectories in the event of a failure. Numerical simulations presented in the paper, both for nominal conditions and for a scenario with a rudder stuck fault, are used to show the utility of the authors' method.

Kluever [10] developed an A&L guidance method based on trajectory planning. Kluever's method involved computing a desirable reference trajectory online that brings the RLV from its initial state to a desired landing condition by piecing together several flight segments. An iterative method determined the quasi-equilibrium glideslope for a constant dynamic pressure, and then a backward trajectory propagation method adjusted the flight-path angle such that dynamic pressure was matched at the pull-up altitude. Results were presented that showed that the trajectory-planning method is able to generate feasible reference trajectories very quickly, even with the addition of variations in wind and vehicle drag. Kluever [11] later applied his trajectory-planning approach for the case of a RLV with damaged control surfaces. The damaged control surfaces scenario was modeled by placing a limit on the normal acceleration capabilities. Through a set of optimization trials, Kluever developed a method for generating feasible trajectories by using a constant load factor of 1.1 g for the entire trajectory. With this approach, a small but constant normal acceleration is applied that continuously rotates the flight-path angle upward. Results were presented that showed that the generated trajectories satisfy the condition of a near-zero vertical velocity at touchdown, with the desired touchdown position being missed by 300 ft.

This paper presents a novel method for generating online A&L trajectories by taking advantage of the finite-time-reaching phase of the sliding mode control technique. The only information the control law requires in addition to the instantaneous state of the system is the desired runway location and the A&L initial conditions. Thus, a certain level of robustness to initial conditions is obtained. Note that this study is not meant to address problems with impaired vehicles. To solve this problem, a concept of sliding mode terminal guidance (SMTG) is used. In SMTG the sliding surface is chosen as a terminal constraint, which is the altitude at the landing site in this case. Then, by making use of the finite-time-reaching phase of sliding mode, it can be guaranteed that the terminal constraint will be reached in a finite time. A key principle in these types of problems is that once the sliding surface is reached, the problem is complete, and so no movement along the sliding surface is required. It should be noted that while there have been previous approaches to reentry guidance with the sliding mode technique [12,13], these approaches involved tracking a trajectory generated offline and *not* creation of new trajectories to adapt to current conditions.

System Model and Equations of Motion

This section details the system model of an RLV during the approach and landing phase. It is assumed that the scenario is conducted entirely in a vertical plane or, in other words, that the initial crossrange to the runway is zero. For reference, a diagram of the A&L phase can be found in Fig. 1.

The equations of motion of an unpowered RLV during the A&L phase are

$$\dot{V} = -\frac{D}{m} - g\sin\gamma \tag{1}$$

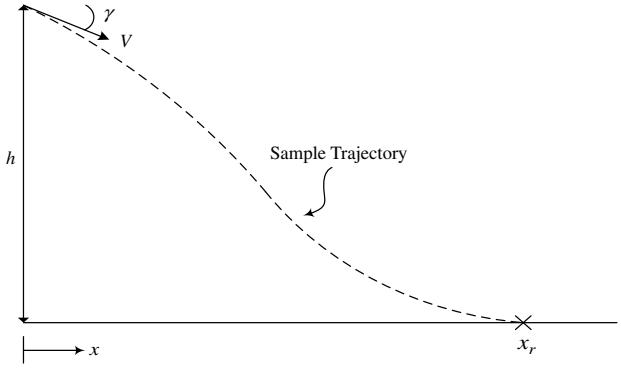

Fig. 1 Diagram of the approach and landing phase.

$$\dot{\gamma} = \frac{L}{mV} - \frac{g\cos\gamma}{V} \tag{2}$$

$$\dot{h} = V\sin\gamma \tag{3}$$

$$\dot{x} = V\cos\gamma \tag{4}$$

In Eqs. (1) and (2), the lift and drag forces are defined as

$$L = \bar{q}SC_L \tag{5}$$

$$D = \bar{q}SC_D \tag{6}$$

where $\bar{q} = \frac{1}{2}\rho V^2$ is the dynamic pressure. An exponential air density profile is assumed as

$$\rho = \rho_0 e^{-(h/H)} \tag{7}$$

and the lift and drag coefficients take the form of

$$C_L = C_{L_0}\sin^2\alpha\cos\alpha \tag{8}$$

$$C_D = C_{D_0} + KC_L^2 \tag{9}$$

The values of the parameters used in Eqs. (1–9) can be found in Table 1.

The equations of motion (1–4) are used for the guidance law development detailed in the next section, in which the derivative of the lift coefficient, $\dot{C}_L$, is taken as the control input.

Reentry SMTG Design

This section covers the development of SMTG and its application to the A&L reentry phase and consists of two parts. First, a general approach for solving sliding mode problems with a relative degree of 2 is derived. Afterwards, the steps in the use of this approach for solving the A&L guidance problem are given.

Sliding Mode Control for Systems with Relative Degree of 2

It is well known that first-order sliding mode approaches can only be used when the sliding surface has a relative degree of 1 [14]. To

Table 1 RLV parameters

Parameter	Value
S/m	0.91177458 ft^2/slug
C_{L_0}	2.3
C_{D_0}	0.0975
K	0.1819

handle problems with larger relative degrees, a higher-order sliding mode (HOSM) approach must be used. In HOSM, both the sliding surface and its successive derivatives are driven to zero: that is,

$$s, \dot{s}, \ddot{s}, \ldots s^{(r-1)} = 0$$

where r is the relative degree. Most HOSM algorithms are of the second order and can be used to either handle problems with a relative degree of 2 or to reduce chattering in problems with a relative degree of 1. One of the more popular second-order sliding mode approaches is the twisting algorithm [15], in which the sliding surface and its derivative make an infinite number of rotations (twists) about the origin and reach zero in a finite time. Although the twisting algorithm is a very useful approach that has been used for a variety of applications [16–19], since it forces the sliding surface to oscillate between positive and negative values before converging to zero, there are certain applications for which it *cannot* be used. In particular, the twisting algorithm cannot be used for certain terminal sliding mode problems, in which once the sliding surface crosses zero, the problem is generally considered to be over. Thus, there is a need for a new second-order sliding mode approach that can be used to solve these types of problems. In this section, a novel second-order sliding mode method based on an adaptive backstepping approach is derived. The usefulness of this method is that it guarantees the sliding surface and its derivative will go to zero in a finite time, *while also ensuring that the sliding surface will not cross zero until the final time*.

First assume that is desired to reach a sliding surface of the form

$$s_1 = f(\mathbf{x}) = 0 \tag{10}$$

and that the first two time derivatives of s_1 are

$$\dot{s}_1 = h(\mathbf{x}) \tag{11}$$

$$\ddot{s}_1 = l(\mathbf{x}) + g(\mathbf{x})u \tag{12}$$

The functions $h(\mathbf{x})$, $l(\mathbf{x})$, and $g(\mathbf{x})$ are assumed to be known functions of $\mathbf{x}$, the state vector. It can be seen that the control input u appears in the second derivative of the sliding surface, so the surface s_1 has a relative degree of 2.

The goal is to find an expression for u such that the sliding surface s_1 and its derivative $\dot{s}_1$ will both go to zero at some desired finite time t_r. This goal is achieved through the use of a backstepping approach, where $\dot{s}_1$ is taken as a *virtual* control input. To find the value of $\dot{s}_1$ that would be needed to drive s_1 to zero, a candidate Lyapunov function V_{l_1} is chosen as

$$V_{l_1} = \tfrac{1}{2}s_1^2 \tag{13}$$

Taking the time derivative of Eq. (13) leads to

$$\dot{V}_{l_1} = s_1\dot{s}_1 \tag{14}$$

To guarantee that the surface s_1 will go to zero in a finite time, $\dot{s}_1$ must be chosen such that V_{l_1} is negative-definite. This negative-definite property can be achieved by choosing $\dot{s}_1$ as

$$\dot{s}_1 = -\frac{ns_1}{t_r - t}, \qquad n > 1 \tag{15}$$

Substituting Eq. (15) into (14), it is found that

$$\dot{V}_l = -\frac{ns_1^2}{t_r - t} < 0 \tag{16}$$

Since the Lyapunov function's derivative is negative-definite, Eq. (16) guarantees that the sliding surface will go to zero at the desired finite time t_r. Also, note that Eq. (16) is an *adaptive* term in that it changes in magnitude and adapts to the trajectory the sliding surface is following. An interesting and useful result of this adaptive approach is that it can *also* be guaranteed that $\dot{s}_1$ will go to zero at t_r. A proof of this result can be found in the Appendix.

Equation (15) essentially defines a desired trajectory for the sliding surface's derivative to follow. Obviously, the condition of Eq. (15) will not necessarily be met at the initial time, as the initial value of $\dot{s}_1$ depends entirely on the initial conditions of the problem. Thus, the control input u must be used to drive $\dot{s}_1$ from its initial value to the trajectory defined by Eq. (15) in a finite time and then keep $\dot{s}_1$ on that trajectory. Since the system must perform some movement along the trajectory of Eq. (15) to guarantee that s_1 and $\dot{s}_1$ will go to zero, it is important that the trajectory be reached some finite amount of time *before* the reaching time t_r.

One way to guarantee that the desired trajectory will be reached in a finite time is to consider Eq. (15) as a *new* sliding surface:

$$s_2 = \dot{s}_1 + \frac{ns_1}{t_r - t} = 0 \tag{17}$$

The time derivative of the surface s_2 can then be found as

$$\dot{s}_2 = l(\mathbf{x}) + \frac{n\dot{s}_1(t_r - t) + ns_1}{(t_r - t)^2} + g(\mathbf{x})u \tag{18}$$

It can be seen from Eq. (18) that the new sliding surface s_2 has a relative degree of one with respect to the control input u.

To find an expression for u that will drive s_2 to zero in some finite time t_r^*, a candidate Lyapunov function is chosen as

$$V_{l_2} = \tfrac{1}{2}s_2^2 \tag{19}$$

Differentiating Eq. (19) leads to

$$\dot{V}_{l_2} = s_2\dot{s}_2 = s_2\left[l(\mathbf{x}) + \frac{n\dot{s}_1(t_r - t) + ns_1}{(t_r - t)^2} + g(\mathbf{x})u\right] \tag{20}$$

To make Eq. (20) negative-definite, u is selected as

$$u = -\frac{1}{g(\mathbf{x})}\left[l(\mathbf{y}) + \frac{n\dot{s}_1(t_r - t) + ns_1}{(t_r - t)^2} + \eta\,\mathrm{sgn}\left(\dot{s}_1 + \frac{ns_1}{t_r - t}\right)\right] \tag{21}$$

In Eq. (21), the η term is a positive constant that defines how quickly the surface s_2 will go to zero.

To achieve a particular finite reaching time t_r^* for s_2, η is chosen as

$$\eta = \frac{|s_2(0)|}{t_r^*} \tag{22}$$

where $s_2(0)$ is the initial value of s_2. For the sliding surface s_1 and its derivative $\dot{s}_1$ to go to zero exactly at the finite time t_r, it is important that the surface s_2 go to zero *before* t_r. A necessary condition for the convergence of s_1 and $\dot{s}_1$ is thus

$$t_r^* < t_r \tag{23}$$

If this condition is satisfied, the control law of Eq. (21) guarantees that s_2 will go to zero in the finite time t_r^*, and s_1 and $\dot{s}_1$ will to go to zero in the finite time t_r.

The results from this analysis can be summarized in the following theorem:

Theorem 1: Suppose a sliding surface $s = f(\mathbf{x})$ has a relative degree of 2, with a second derivative of the form $\ddot{s} = l(\mathbf{x}) + g(\mathbf{x})u$. Then, using the control law

$$u = -\frac{1}{g(\mathbf{x})}\left[l(\mathbf{x}) + \frac{n\dot{s}(t_r - t) + ns}{(t_r - t)^2} + \frac{|\dot{s}(0) + \frac{ns(0)}{t_r - t}|}{t_r^*}\,\mathrm{sgn}\left(\dot{s} + \frac{ns}{t_r - t}\right)\right] \tag{24}$$

it can be guaranteed that s and $\dot{s}$ will go to zero in the finite time t_r, provided $n > 1$ and $t_r^* < t_r$.

A proof of the above theorem can be found in the Appendix.

The control law of Eq. (21) is a very useful result, as it guarantees that the sliding surface and its derivative will go to zero in some

desired finite time. However, due to the adaptive nature of the control law, it *cannot* be used to maintain the system on the surface $s_1, \dot{s}_1 = 0$ after it is reached. This behavior can easily be observed by noting that when $t > t_r$, Eq. (16) is no longer negative-definite. There is thus a limit to the range of problems to which the control law of Eq. (24) can be applied. The proposed control law, however, is an excellent choice for terminal sliding mode problems such as the reentry guidance problem analyzed in this work. It should also be noted that by applying the backstepping approach multiple times, the method presented in this section can be applied for sliding surfaces with arbitrary relative degrees.

In terms of the implementation of Eq. (24), note that since the system performs some movement along the surface s_2, chattering would likely be experienced due to the use of the *signum* function in the control law. To eliminate this chattering effect, a simple saturation function can be used. By using a saturation function, chattering can be virtually eliminated, but this comes at the cost of only achieving guaranteed convergence to a *boundary layer* about the surface $s = 0$. Although it can be guaranteed that the sliding surface will reach the boundary layer and then stay inside its boundaries once it has been reached, no stability guarantees can be provided for the system inside the boundary layer. However, the size of the boundary layer can be controlled by the user. By making the boundary-layer size sufficiently small, the error in the sliding surface can be reduced to negligible values.

Application of SMTG to Reentry Terminal Guidance

This section details the steps in the application of the SMTG method to the reentry terminal guidance problem. For the A&L reentry phase, the two primary terminal constraints are as follows:

1) The RLV must land on a desired runway located at some distance downrange of the entry point of the A&L phase.

2) The RLV must land with a sufficiently small vertical velocity.

The SMTG-based guidance law developed in this section will lead to both of the above objectives being satisfied for a desired runway location relative to the A&L entry point. It should be noted that only longitudinal two-dimensional motion is analyzed in this work. Thus, the vehicle attitude/orientation and any crossrange errors are not considered.

A sliding surface is first chosen to make the final altitude zero as

$$s = h = 0 \tag{25}$$

The sliding surface s is then differentiated until the control input $\dot{C}_L$ appears, giving

$$\dot{s} = \dot{h} = V \sin\gamma \tag{26}$$

$$\ddot{s} = A \tag{27}$$

$$\dddot{s} = B + C\dot{C}_L \tag{28}$$

In Eqs. (27) and (28), the terms A, B, and C are highly nonlinear functions with the expressions

$$A = -g + \frac{1}{2}\rho V^2\left(\frac{S}{m}\right)\left[\cos\gamma C_L - K\sin\gamma C_L^2\right] - \frac{1}{2}\rho V^2\left(\frac{S}{m}\right)\sin\gamma C_{D_0} \tag{29}$$

$$B = \rho V\left(\frac{S}{m}\right)\left[\cos\gamma C_L - K\sin\gamma C_L^2 - \sin\gamma C_{D_0}\right]\dot{V} + \frac{1}{2}\rho V^2\left(\frac{S}{m}\right)\left[-\sin\gamma C_L - K\cos\gamma C_L^2 - \cos\gamma C_{D_0}\right]\dot{\gamma} \tag{30}$$

$$C = \frac{1}{2}\rho V^2\left(\frac{S}{m}\right)[\cos\gamma - 2K\sin\gamma C_L] \tag{31}$$

Equation (28) shows that the control input appears in the third derivative, so the sliding surface s has a relative degree of three. It should be noted that the lift coefficient itself is not used as the control input for this work, because the lift coefficient appears in Eq. (27) in a nonaffine form.

By inspecting Eqs. (25) and (26), it can be seen that the condition $s = \dot{s} = 0$ states that the RLV will be at a zero altitude with a zero vertical velocity. However, a zero vertical velocity at touchdown is unnecessarily restrictive, as the maximum vertical velocity at touchdown for the space shuttle is typically between 7 and 10 ft/s. A more reasonable approach would thus involve constraining the vertical velocity at touchdown to be some specific finite value rather than zero. To allow for this constraint, a *new* variable is defined as

$$\dot{z} = \dot{s} - \dot{s}_{\text{des}} = 0 \tag{32}$$

where

$$\dot{s}_{\text{des}} = \dot{h}_{\text{des}} \tag{33}$$

and $\dot{h}_{\text{des}}$ is the desired vertical velocity at touchdown. It can clearly be seen from Eq. (32) that if $\dot{z}$ is driven to zero, the vertical velocity of the RLV will be equal to its desired value.

Integrating Eq. (32) leads to the expression

$$z = s - \dot{s}_{\text{des}}t + c \tag{34}$$

where c is a constant. Now define a new term, called the *time-to-go*, as

$$t_{\text{go}} = \frac{r}{V} \tag{35}$$

where r is the instantaneous range from the RLV to the runway given by

$$r = \sqrt{(x_r - x)^2 + h^2} \tag{36}$$

The time-to-go gives an approximation of the time it will take the RLV to reach the runway if it follows its present course. Using this time-to-go expression, the term c in Eq. (34) is now chosen as

$$c = \dot{s}_{\text{des}}(t_{\text{go}} - t) \tag{37}$$

Substituting Eq. (37) into Eq. (34) leads to

$$z = s - \dot{s}_{\text{des}}t - \dot{s}_{\text{des}}(t_{\text{go}} - t) \tag{38}$$

Finally, simplifying Eq. (38) and substituting Eqs. (25) and (33), the expression for z becomes

$$z = h + \dot{h}_{\text{des}}t_{\text{go}} \tag{39}$$

Now, suppose that z is driven to zero at the runway. Since the time-to-go, t_{go}, goes to zero as the distance to the runway (i.e. the range r) goes to zero, the second term in Eq. (39) will go to zero at the runway. Thus, in order for Eq. (39) to be zero at the runway, the first term in the equation (h) must *also* be zero. This implies that the altitude will be zero at the runway, satisfying the touchdown requirement.

Equation (39) can be considered as a *new* sliding surface, which satisfies the same property as the original sliding surface in Eq. (25). As was done before, Eq. (39) is now differentiated until the control input appears, leading to

$$\dot{z} = \dot{y} - \dot{y}_{\text{des}} \tag{40}$$

$$\ddot{z} = A \tag{41}$$

$$\dddot{z} = B + C\dot{C}_L \tag{42}$$

where the terms A, B, and C were defined previously. Note from Eq. (42) that, as before, the sliding surface in Eq. (39) has a relative degree of three.

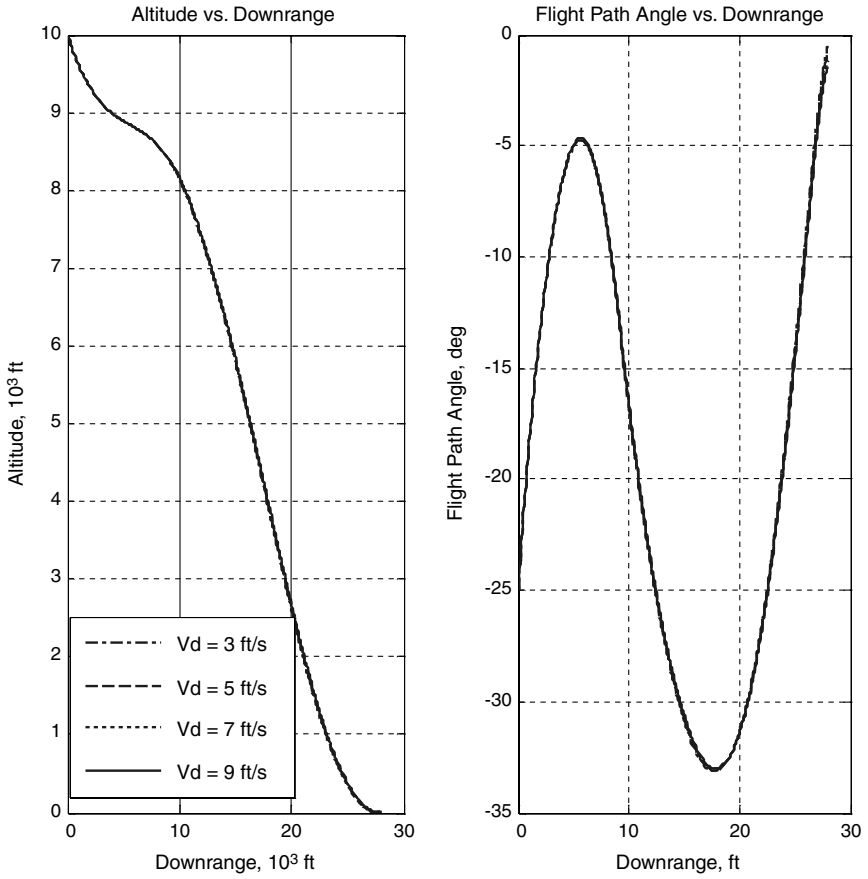

Fig. 2 Altitude and flight-path angle with varying final vertical velocity.

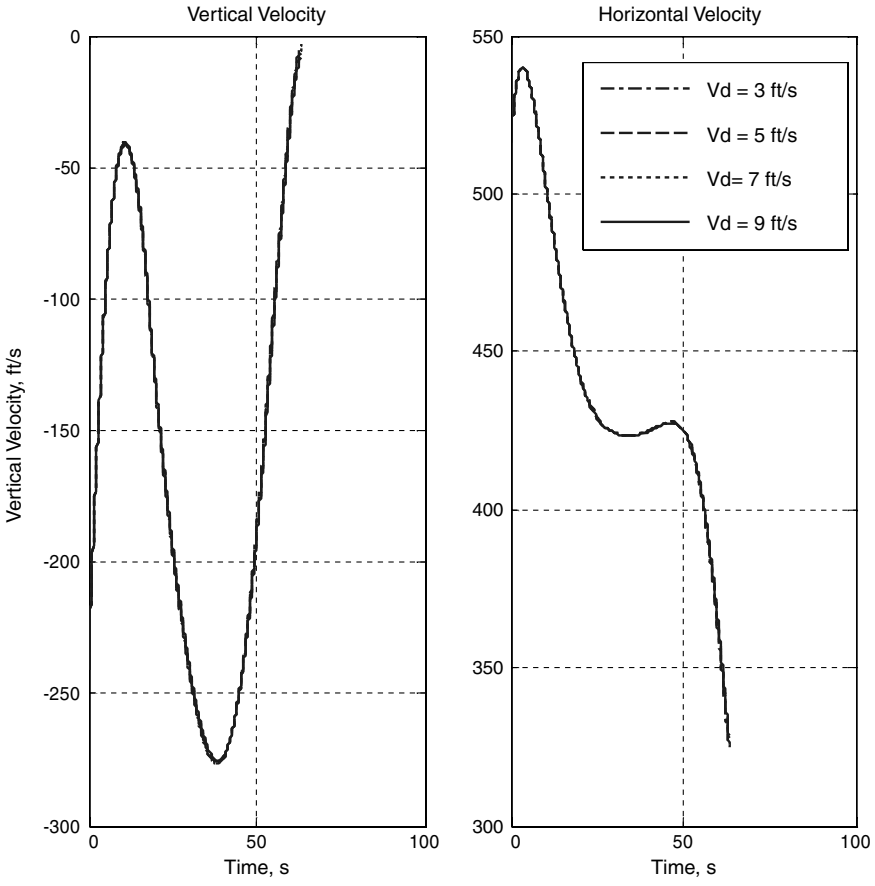

Fig. 3 Vertical and horizontal velocity with varying final vertical velocity.

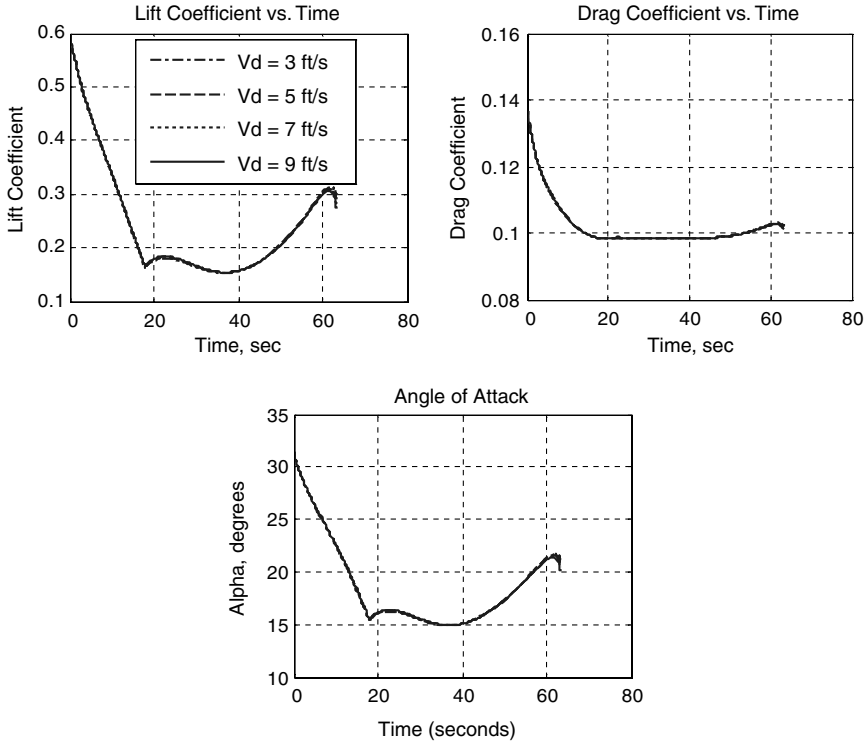

Fig. 4 Lift coefficient, drag coefficient, and angle of attack with varying final vertical velocity.

Note that the condition $z = \dot{z} = 0$ implies that the RLV will be at a zero altitude with the desired amount of vertical velocity. Thus, the reentry guidance problem can be solved by finding an expression for the derivative of the lift coefficient that will guarantee that the sliding surface z and its derivative $\dot{z}$ will go to zero at some desired downrange position x_r corresponding to the runway.

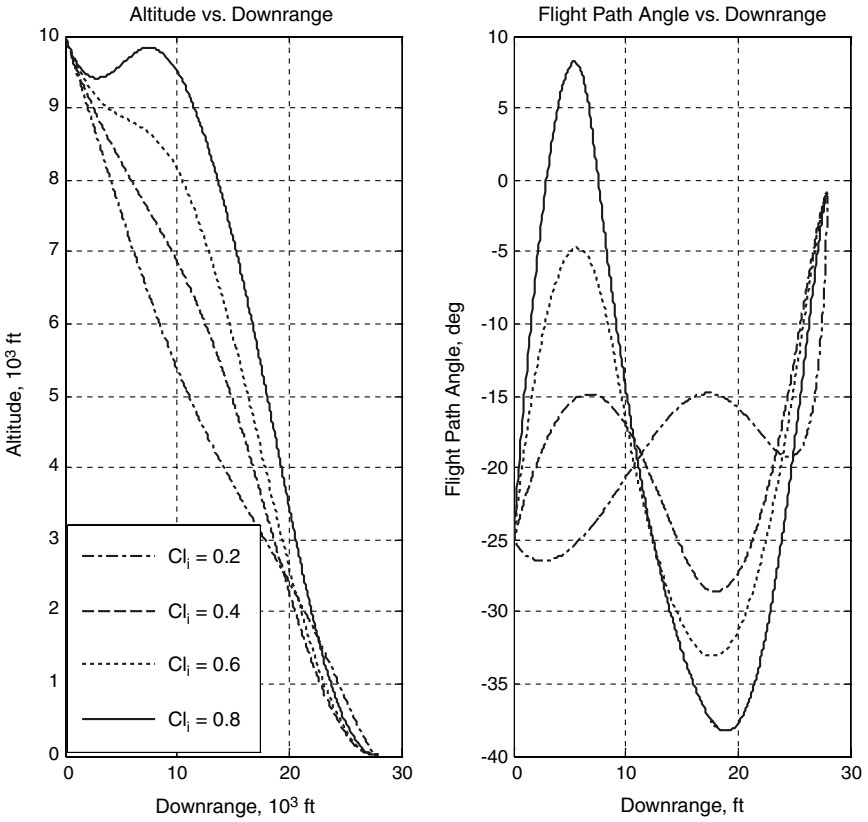

Fig. 5 Altitude and flight-path angle with varying initial lift coefficient.

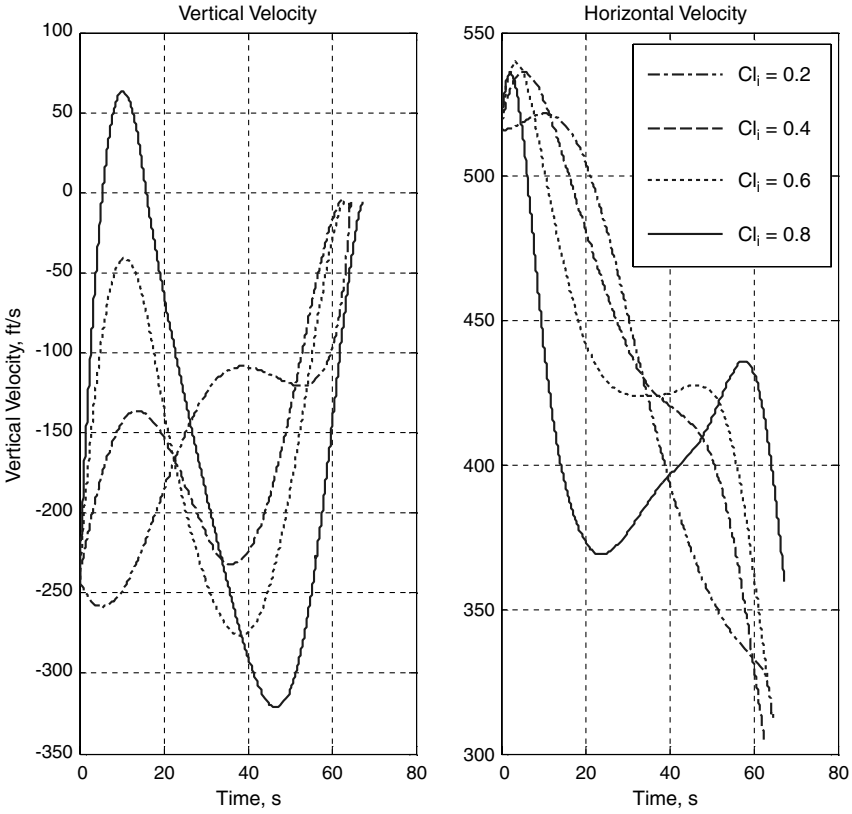

Fig. 6 Vertical and horizontal velocity with varying initial lift coefficient.

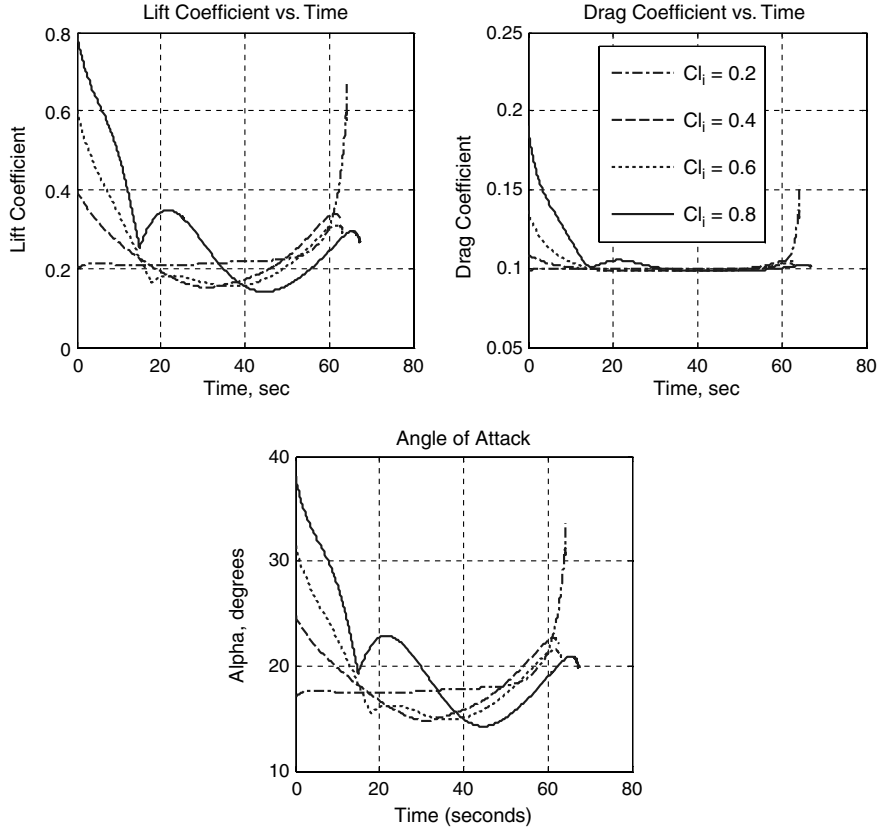

Fig. 7 Lift coefficient, drag coefficient, and angle of attack with varying initial lift coefficient.

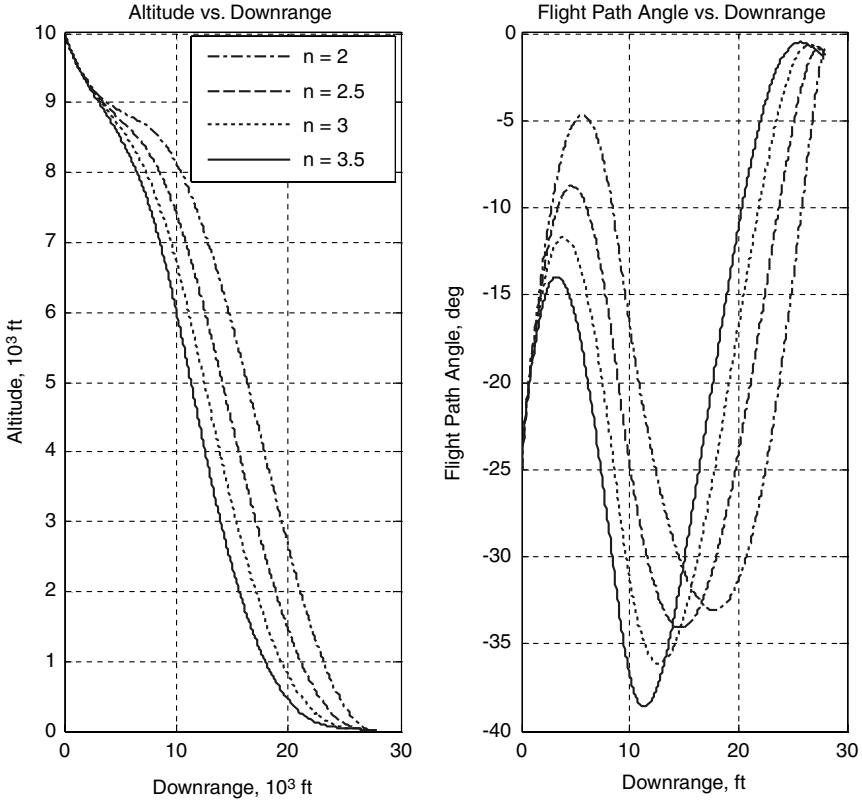

Fig. 8 Altitude and flight-path angle with varying *n*.

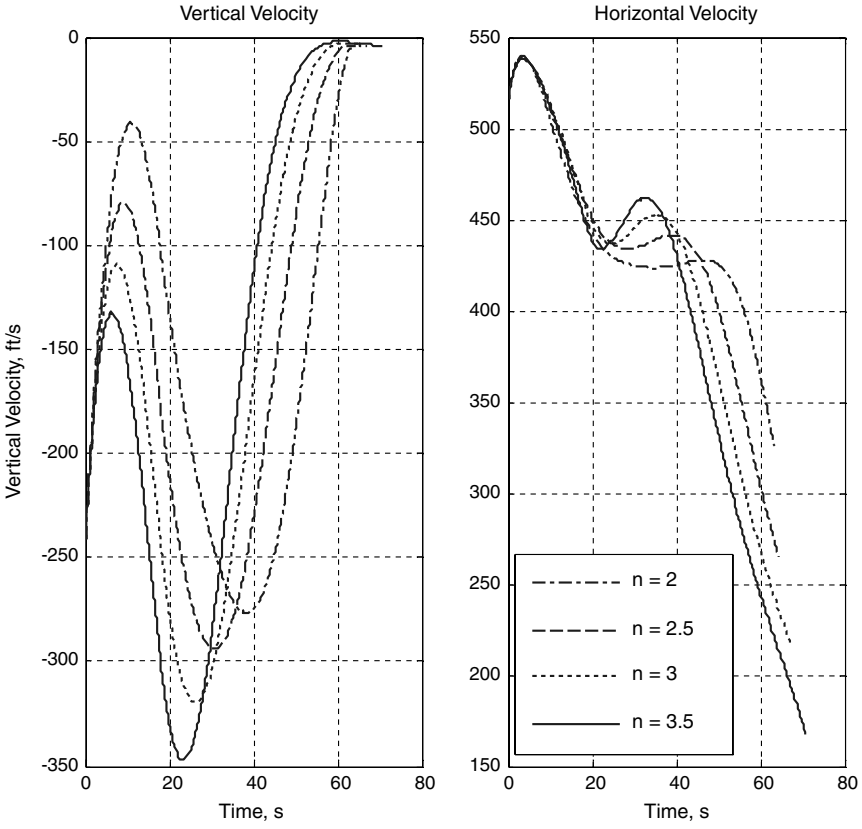

Fig. 9 Vertical and horizontal velocity with varying *n*.

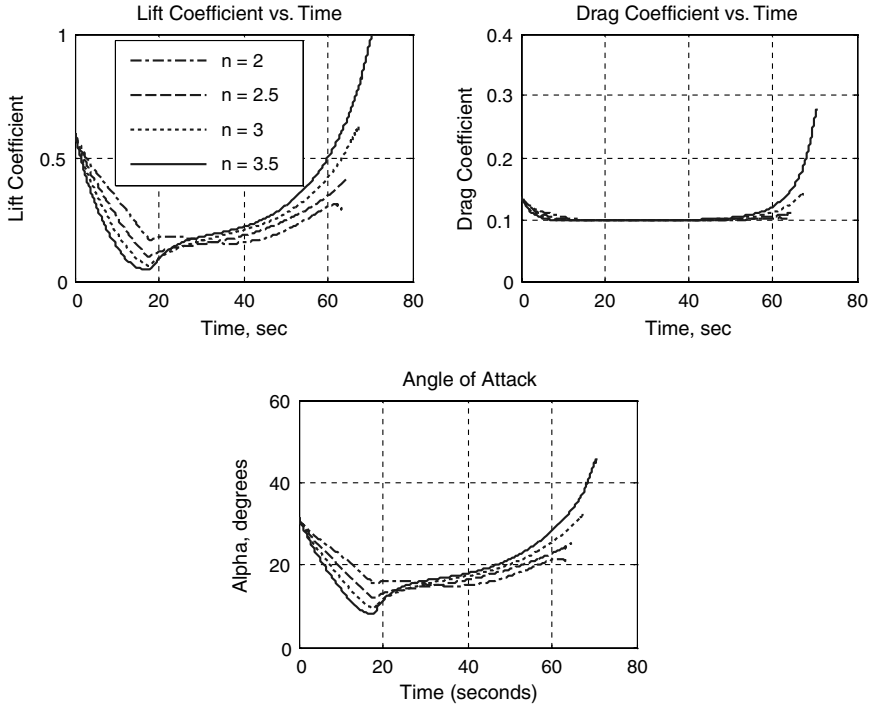

Fig. 10 Lift coefficient, drag coefficient, and angle of attack with varying n.

By applying the backstepping approach from the previous section *twice*, the required lift coefficient derivative is found to be

$$\dot{C}_L = -\frac{1}{C}\left\{ B + \frac{nAt_{\text{go}}^2 + 2n(\dot{y}-\dot{y}_{\text{des}})t_{\text{go}} + 2n(y+\dot{y}_{\text{des}}t_{\text{go}})}{t_{\text{go}}^3} + \frac{n\left[A + \frac{n(\dot{y}-\dot{y}_{\text{des}})t_{\text{go}}+n(y+\dot{y}_{\text{des}}t_{\text{go}})}{t_{\text{go}}^2}\right]t_{\text{go}} + n\left[\dot{y}-\dot{y}_{\text{des}} + \frac{n(y+\dot{y}_{\text{des}}t_{\text{go}})}{t_{\text{go}}}\right]}{t_{\text{go}}^2} + \eta\,\text{sgn}\left(A + \frac{n(\dot{y}-\dot{y}_{\text{des}})t_{\text{go}} + n(y+\dot{y}_{\text{des}}t_{\text{go}})}{t_{\text{go}}^2} + \frac{n\left[\dot{y}-\dot{y}_{\text{des}} + \frac{n(y+\dot{y}_{\text{des}}t_{\text{go}})}{t_{\text{go}}}\right]}{t_{\text{go}}}\right)\right\} \tag{43}$$

where

$$\eta = \frac{\left|A_0 + \frac{n(\dot{y}_0-\dot{y}_{\text{des}})t_{\text{go}_0}+n(y_0+\dot{y}_{\text{des}}t_{\text{go}_0})}{t_{\text{go}_0}^2} + \frac{n[\dot{y}_0-\dot{y}_{\text{des}}+\frac{n(y_0+\dot{y}_{\text{des}}t_{\text{go}_0})}{t_{\text{go}_0}}]}{t_{\text{go}_0}}\right|}{x_r^*} \tag{44}$$

In Eq. (44), the subscript 0 corresponds to the initial value of the respective variable. Also, the variable x_r^* in Eq. (44) is similar to the variable t_r^* in Eq. (24). Thus, a necessary condition for the convergence of z and $\dot{z}$ to zero at x_r is

$$x_r^* < x_r \tag{45}$$

Also, in order to eliminate the chattering effect, the *signum* function is replaced with a *saturation* function when implementing the control law of Eq. (43). The boundary-layer size for the saturation function was chosen as $\varepsilon = 1\text{e}-3$. It should be noted that Eq. (43) is a feasible approach to calculating the lift coefficient derivative only when the longitudinal motion problem is being analyzed. If motion in three dimensions was considered, additional lift functional dependencies would need to be included.

Note from the structure of the control law in Eq. (43) that two tuning parameters are available to shape the trajectories: the constant n and the initial lift coefficient. Although the control law will allow for the RLV to touchdown on the runway with a desired velocity for any combination of these two parameters (provided $n > 1$), the resulting trajectory and the transient performance will vary depending on the particular combination of tuning parameters. A chart for choosing the combination of tuning parameters that provides for acceptable performance is provided in the next section.

In many scenarios, it is also desired to know how the angle of attack α of the RLV is changing as the mission progresses. Given the instantaneous value of the lift coefficient, the angle of attack can be calculated using Eq. (8). Since Eq. (8) is a nonlinear equation, Newton's method is used to solve for α. The value of α at the *previous* time serves as a good initial in implementing Newton's method (since the goal is for an online implementation), when calculating α for a particular point in time.

There are a variety of ways in which the control law of Eq. (43) could be implemented in a reusable launch vehicle. First, Eq. (42) could be used to provide values of the lift coefficient that could be tracked online. Another (possibly more realistic) approach would be to solve Eq. (8) for the angle of attack α. Once α is known and is acceptable, some other kinematic variable could be used for tracking.

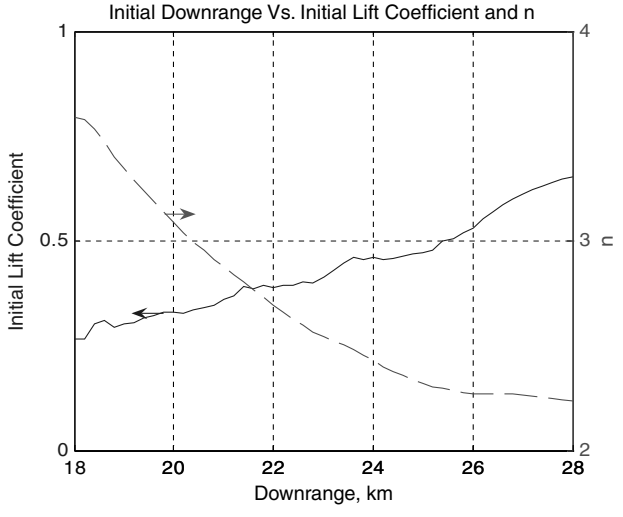

Fig. 11 Initial lift coefficient and n as a function of initial downrange.

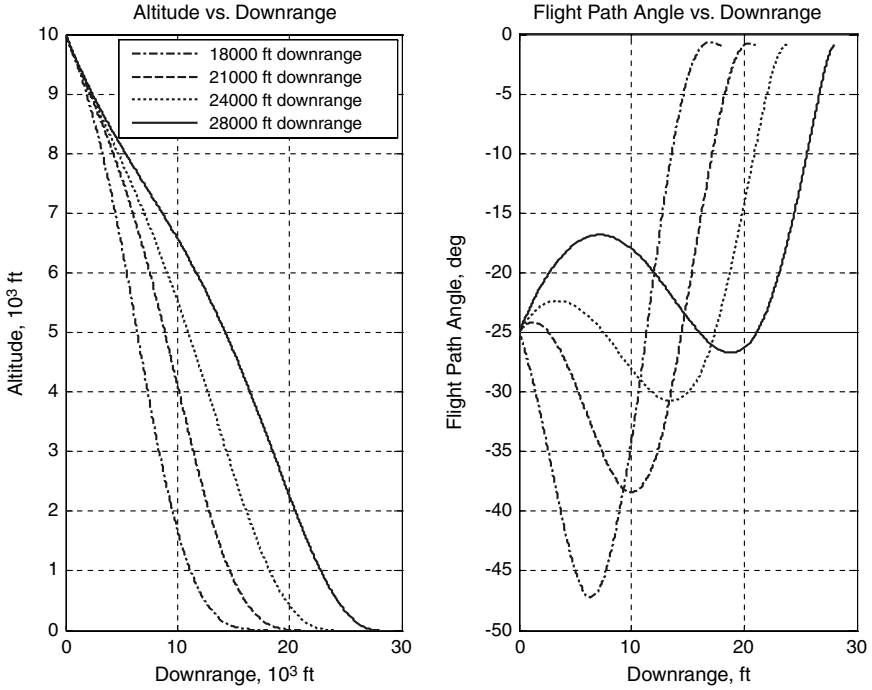

Fig. 12 Altitude and flight-path-angle histories with varying initial downrange.

Results and Analysis

In this section, simulations of the proposed reentry guidance approach will be presented. For each of these simulations, the initial values for the altitude, velocity, and flight-path angle are taken as 10,000 ft, 570 ft/s, and -25° respectively.

First, it was desired to see the effect of varying the desired vertical velocity at touchdown, initial lift coefficient, and value for n in Eq. (43). To analyze these effects, a set of simulations were performed for an initial downrange of 28,000 ft. In all of these simulations, the value of x_r^* in Eq. (44) is taken as

$$x_r^* = 0.2x_r \tag{46}$$

This value of x_r^* was found to yield acceptable results, but it should be noted that many other values could be chosen as well. Figures 2–4 contain the results of a simulation of varying the desired vertical velocity at touchdown for a specific initial lift coefficient and n of 0.6 and 2, respectively. Next, Figs. 5–7 show the outcome of varying the initial lift coefficient for a set desired vertical velocity at touchdown and n of 5 ft/s and 2, respectively. Finally, results obtained from varying n for specific initial lift coefficient and desired vertical velocity at touchdown velocities values of 0.6 and 5 ft/s, respectively, can be found in Figs. 8–10.

Inspecting the results of varying the desired vertical velocity at touchdown in Figs. 2–4, it is interesting to observe that the final vertical velocity has a fairly negligible effect on the resulting trajectories. However, Figs. 5–10 clearly show that the values of the initial lift coefficient and n have a large impact on the transient performance and nature of the trajectories. From Fig. 5, it is noted that by increasing the lift coefficient, the RLV begins to perform an increasingly large pull-up maneuver at the beginning of the trajectory. The flight-path angle at touchdown is roughly 1.2° for each initial lift coefficient case. Also, as shown in Fig. 6, while each initial lift coefficient satisfies the desired vertical velocity condition of 5 ft/s at touchdown, the horizontal velocity at touchdown increases as the initial lift coefficient increases. Finally, Fig. 7 indicates the result that the lift coefficient, drag coefficient, and angle of attack at touchdown tend to decrease as the lift coefficient as increased. In terms of the parameter n, note from Fig. 8 that as n is increased, there is a more gradual decrease in the flight-path angle as

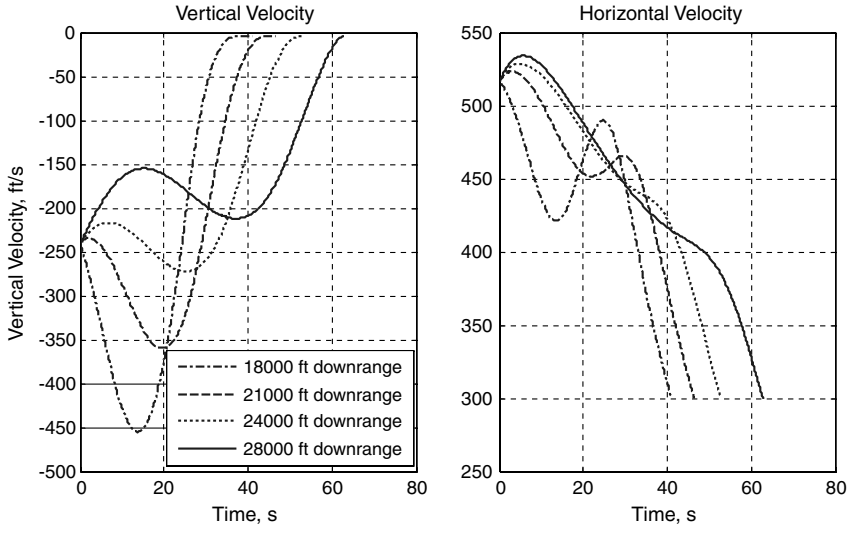

Fig. 13 Vertical and horizontal velocity histories with varying initial downrange.

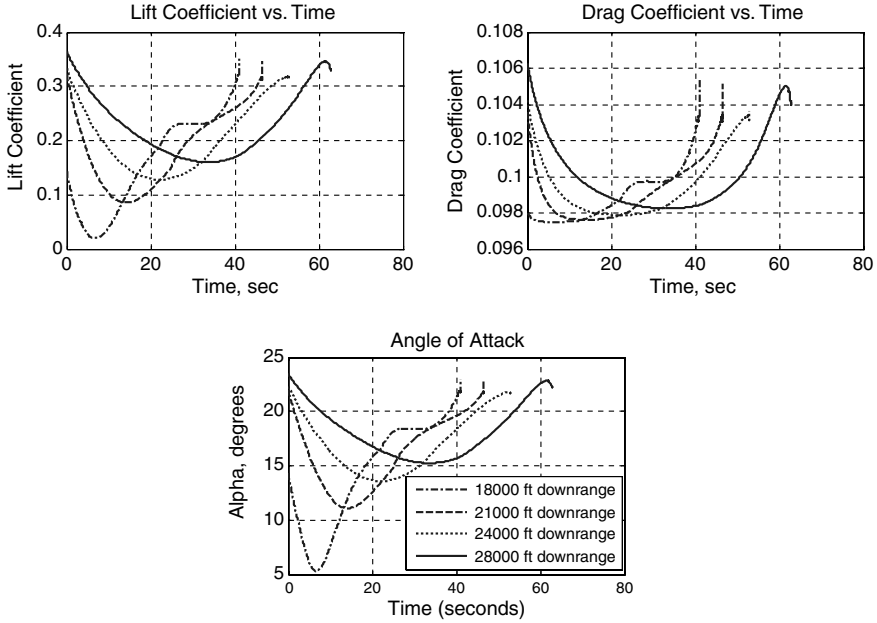

Fig. 14 Lift coefficient, drag coefficient, and angle-of-attack histories with varying initial downrange.

the RLV approaches the runway. The gradual decrease in the flight-path angle near the runway is similar to the flare maneuver that is typically desired before touchdown. Further, Fig. 9 shows that the horizontal velocity at touchdown decreases as the value of n increases. Because of this behavior, as expected the lift coefficient, drag coefficient, and angle of attack at touchdown from Fig. 10 appear to increase as the value of n increases. From these results, it appears that for a downrange of 28,000 ft, a high initial lift coefficient and a low value of n lead to acceptable transient performance.

To help with picking suitable values for the initial lift coefficient and the parameter n as the initial downrange is changed, a study was performed to investigate how the required initial lift coefficient and n evolve as the initial downrange is increased. To perform this analysis, a large number of simulations were performed to characterize the desired initial lift coefficient and n for various values of the initial downrange. In these simulations, the two parameters were tuned to satisfy the condition that the final horizontal velocity be roughly 300 ft/s. It was found that a horizontal velocity at touchdown of this magnitude leads to fairly acceptable values for the final lift coefficient, drag coefficient, and angle of attack. The results of this analysis are given in Fig. 11.

In Fig. 11, the solid trajectory corresponds to the required initial lift coefficient, and the dashed trajectory corresponds to the required value for n. The lift coefficient values are read off of the left-hand side of the plot, and the values of n are found on the right-hand side. The usefulness of Fig. 11 is that for any particular value for the initial downrange, the plot can be used to immediately find the required values for the initial lift coefficient and n. For example, Fig. 11 indicates that for an initial downrange of 20,000 ft, one should use an initial lift coefficient of roughly 0.39 and a value for n of roughly 3.2. Thus, Fig. 11 can be considered as a guide for selecting the tuning parameters as the initial downrange changes. Note from Fig. 11 the interesting trend that as the initial downrange increases, the required initial lift coefficient increases and the required value for n decreases.

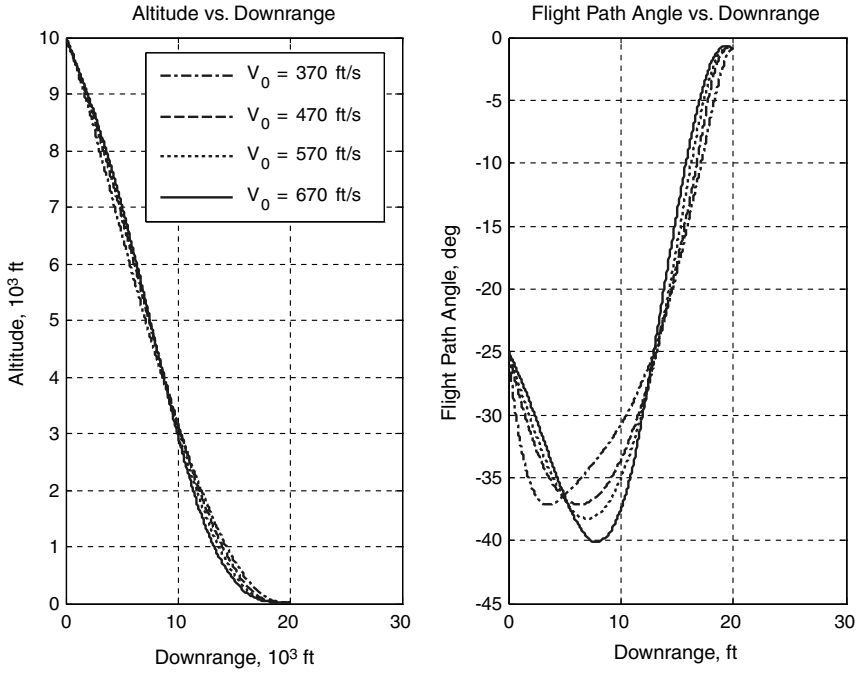

Fig. 15 Altitude and flight-path-angle histories with varying initial velocity.

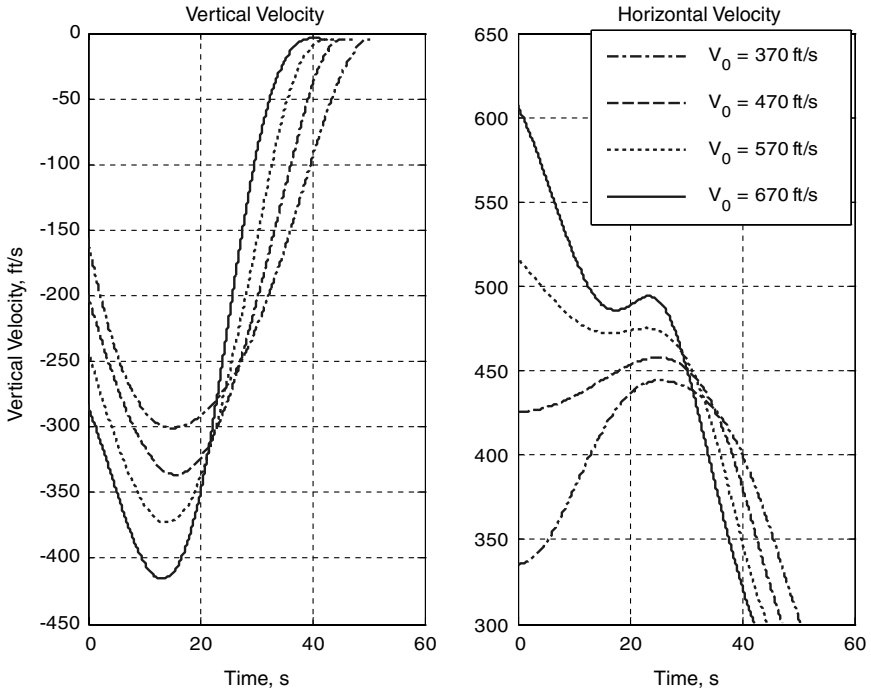

Fig. 16 Vertical and horizontal velocity histories with varying initial velocity.

The next set of simulations involves using the plot in Fig. 11 to test a wide range of initial downrange positions. In particular, simulations were performed with 18,000, 21,000, 24,000, and 28,000 ft for the initial downrange. The goal of this analysis is to show that the SMTG approach can generate feasible trajectories to multiple downrange locations and can account for a range of possible errors in the initial downrange. For each case studied, the desired vertical velocity touchdown is specified as 5 ft/s, and the initial lift coefficient and n are chosen from Fig. 11. The results for this set of simulations can be found in Figs. 12–14.

From Fig. 12, it easy to note that for each downrange location studied, the altitude and flight-path angle are sent to zero at the desired location. Further, for the 18,000 and 21,000 ft downrange cases, the RLV performs an initial pitch-up maneuver, whereas for the 24,000 and 28,000 ft cases, the RLV performs an initial pitch-down maneuver. For each case, the flight-path angle at touchdown is roughly 0.9°.

The vertical velocity histories in Fig. 13 show that the final vertical velocity is 5 ft/s as desired for each initial downrange case. Also, for each case the horizontal velocity at touchdown is roughly 300 ft/s. This is an expected result, as the initial lift coefficient and n values were chosen from Fig. 11. Finally, Fig. 14 shows that the angle of attack and the lift and drag coefficients stay within safe levels for each scenario. The maximum values of the angle of attack, lift coefficient, and drag coefficient are found to be approximately 23, 0.37, and 0.105°, with the largest values being seen near touchdown. It makes intuitive sense that the largest values are seen near touchdown, since for the smaller velocities near touchdown, the RLV must fly at a larger angle of attack to support its weight.

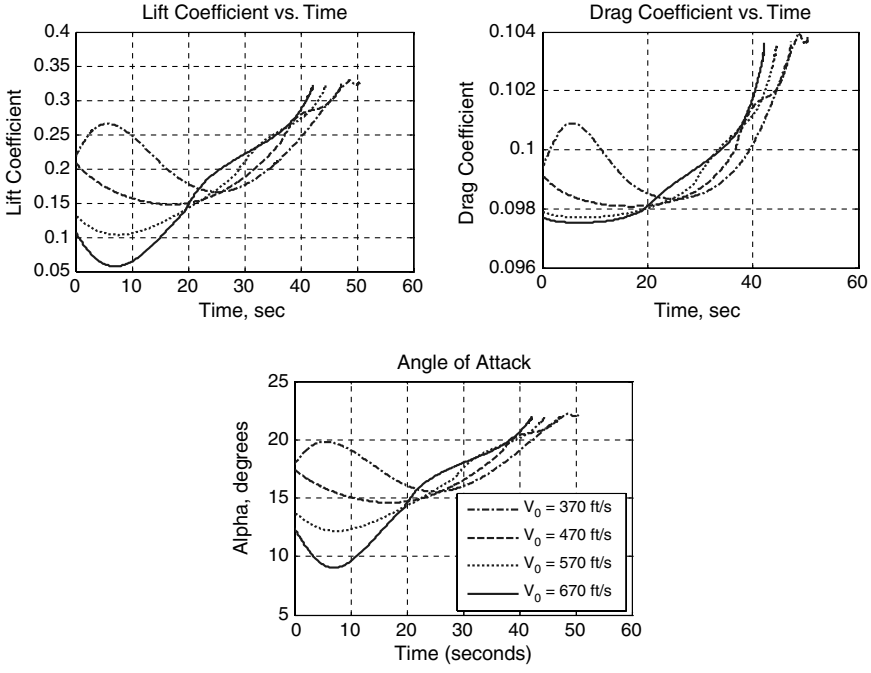

Fig. 17 Lift coefficient, drag coefficient, and angle-of-attack histories with varying initial velocity.

A final set of simulations was performed that involves testing a range of initial velocities for a specific initial downrange of 20,000 ft. Simulations were performed with initial velocities of 370, 470, 570, and 670 ft/s. The results from this set of simulations can be found in Figs. 15–17.

A plot of the altitude and flight-path-angle histories vs downrange is shown in Fig. 15. From this figure, it can clearly be seen that for each value of the initial velocity, a trajectory is generated that drives the altitude to zero and the flight-path angle to roughly 1° in 20,000 ft, as desired. It is noted that varying the initial velocity appears to have a relatively small effect on the resulting altitude and flight-path-angle histories. Next, from an inspection of Fig. 16, the final vertical and horizontal velocities for each initial velocity case are 5 and roughly 300 ft/s, as desired. It is observed form the horizontal velocity histories that for the 370 and 470 ft/s initial velocity cases, the velocity performs an initial *increase*, whereas for the 570 and 670 ft/s cases the velocity performs an initial *decrease*. Finally, the lift coefficient, drag coefficient, and angle-of-attack histories can be found in Fig. 17. For each initial velocity case, it is noted that the lift coefficient, drag coefficient, and angle of attack all stay within acceptable bounds. The maximum values for the lift coefficient, drag coefficient, and angle of attack are found to be roughly 0.33, 0.104, and 22°, respectively.

Conclusions

A method for A&L reentry phase guidance has been introduced through a concept of sliding mode terminal guidance (SMTG). A control law is obtained that allows for the rapid construction of feasible trajectories that depend only on the instantaneous states of the system and the initial and final conditions of the A&L phase. Thus, the availability of a predetermined reference trajectory is not required. Through a set of simulations, it was shown that the approach shows some robustness with respect to variations in the initial downrange and velocity.

Simulations presented for an assortment of A&L reentry scenarios show the usefulness of the SMTG method for generating a feasible landing trajectory. A series of downrange locations and initial velocities were tested, and for each case, the RLV was able to land exactly on the desired runway with a desired vertical velocity. Also, the various aerodynamic and body parameters stayed within safe limits.

It should be further pointed out that this technique can also be used easily for trajectory-shaping design and analysis in offline studies.

Appendix: Proof of the Result in Theorem 1

Assume that a sliding surface is chosen as

$$s = f(x) = 0 \tag{A1}$$

and that the first two time derivatives of the surface (A1) are

$$\dot{s} = h(x) \tag{A2}$$

$$\ddot{s} = l(x) + g(x)u \tag{A3}$$

Consider the control law

$$\dot{s} = -\frac{ns}{t_r - t} \tag{A4}$$

where t_r is the desired reaching time for the sliding surface in Eq. (A1). The control law in Eq. (A4) specifies a constraint on the sliding surface derivative that will not necessarily be satisfied at the initial time. As proven in the paper, a second-order sliding mode control law can be found such that the constraint (A4) can be met in some finite time t_r^*, which is less than t_r. Now assume that at the time t_r^*, the sliding surface of Eq. (A1) is equal to some finite value s^*. At that point, the system (A1–A3) satisfies the constraint in Eq. (A4). Rearranging variables, Eq. (A4) can be rewritten as

$$\frac{ds}{s} = -n\frac{dt}{t_r - t} \tag{A5}$$

Now Eq. (A5) can be integrated from the point (s^*, t_r^*) to some later point (s, t), yielding

$$\ell_n\left(\frac{s}{s^*}\right) = n\,\ell_n\left(\frac{t_r - t}{t_r - t_r^*}\right) = \ell_n\left[\left(\frac{t_r - t}{t_r - t_r^*}\right)^n\right] \tag{A6}$$

Taking the exponential of both sides of Eq. (A6), an analytic equation for s can be found as

$$s = \frac{s^*}{(t_r - t_r^*)^n}(t_r - t)^n = \beta(t_r - t)^n \tag{A7}$$

where β is a constant

$$\beta = \frac{s^*}{(t_r - t_r^*)^n} \tag{A8}$$

Finally, differentiating Eq. (A7), an analytic equation for $\dot{s}$ can be found as

$$\dot{s} = -n\beta(t_r - t)^{n-1} \tag{A9}$$

Equations (A7) and (A9) are analytic expressions for the sliding surface and its derivative after the finite time t_r^* has been reached. Now, inspecting these equations, it can be seen that s and $\dot{s}$ will have a certain behavior as the time t approaches the reaching time t_r depending on the value chosen for n. First, it can be seen from Eq. (A7) that as long as n is greater than zero, the sliding surface will go to zero at the desired reaching time. The primary dependence on n is seen when analyzing the behavior of $\dot{s}$. If n is less than one, Eq. (A9) exhibits a singularity as the reaching time is approached, an obviously undesired result. By setting n equal to one, it can be seen that $\dot{s}$ no longer exhibits a singularity, but instead converges to a constant (β). For this value of n, the system (A1–A3) would exhibit a behavior that is characteristic to a traditional first-order sliding mode control law. If n is set to be *greater* than one, Eq. (A9) shows that the flight-path angle will go to zero as the reaching time is approached. Thus, as long as n is selected to be greater than one, it can be guaranteed that the sliding surface and its derivative will go to zero at the desired reaching time.

References

[1] Hanson, J., "A Plan for Advanced Guidance and Control Technology for 2nd Generation Reusable Launch Vehicles," AIAA Paper 2002-4557, Aug. 2002.

[2] *Entry Guidance Training Manual*, ENT Guid 2102, NASA, Mission Operations Directorate, Training Division, Flight Training Branch, July 1988.

[3] Schierman, J., Ward, D., Monaco, J., and Hull, J., "A Reconfigurable Guidance Approach for Reusable Launch Vehicles," AIAA Paper 2001-4429, Aug. 2001.

[4] Schierman, J., Hull, J., and Ward, D., "Adaptive Guidance with Trajectory Reshaping for Reusable Launch Vehicles," AIAA Paper 2002-4458, Aug. 2002.

[5] Schierman, J., Hull, J., and Ward, D., "Online Trajectory Command Reshaping for Reusable Launch Vehicles," AIAA Paper 2003-5439, Aug. 2003.

[6] Schierman, J., Ward, D., Hull, J., Gahndi, N., Oppenheimer, M., and Doman, D., "Integrated Adaptive Guidance and Control for Re-Entry Vehicles with Flight-Test Results," *Journal of Guidance, Control, and Dynamics*, Vol. 27, No. 6, Nov.–Dec. 2004, pp. 975–988. doi:10.2514/1.10344

[7] Schierman, J., and Hull, J., "In-Flight Entry Trajectory Optimization for Reusable Launch Vehicles," AIAA Paper 2005-6434, Aug. 2005.

[8] Bollino, K., Ross, M., and Doman, D., "Optimal Nonlinear Feedback Guidance for Reentry Vehicles," AIAA Paper 2006-6074, Aug. 2006.

[9] Fahroo, F., and Doman, D., "A Direct Method for Approach and Landing Trajectory Reshaping with Failure Effect Estimation," AIAA Paper 2004-4772, Aug. 2004.

[10] Kluever, C. A., "Unpowered Approach and Landing Guidance Using

Trajectory Planning," *Journal of Guidance, Control, and Dynamics*, Vol. 27, No. 6, Nov. 2004, pp. 967–974. doi:10.2514/1.7877

[11] Kluever, C. A., "Unpowered Approach and Landing Guidance with Normal Acceleration Limits," *Journal of Guidance, Control, and Dynamics*, Vol. 30, No. 3, 2007, pp. 882–885. doi:10.2514/1.28081

[12] Shtessel, Y., and Krupp, D., "Reusable Launch Vehicle Trajectory Control in Sliding Modes," *Proceedings of the American Control Conference*, Inst. of Electrical and Electronics Engineers, Piscataway, NJ, June 1997, pp. 2557–2561.

[13] Shtessel, Y., McDuffie, J., Jackson, M., Gallaher, M., Krupp, D., Hendrix, N., "Sliding Mode Control of the X-33 Vehicle in Launch and Re-Entry Modes," AIAA Paper 1998-4414, Aug. 1998.

[14] Levant, A., "Construction Principles of 2-Sliding Mode Design," *Automatica*, Vol. 43, No. 4, 2007, pp. 576–586. doi:10.1016/j.automatica.2006.10.008

[15] Levant, A., "Sliding Order and Sliding Accuracy in Sliding Mode Control," *International Journal of Control*, Vol. 58, No. 6, 1993, pp. 1247–1263.

[16] Horn, M., and Reichhartinger, M., "Second-Order Sliding Mode Control of Electronic Throttle Valves," *Proceedings of the International Workshop on Variable Structure Systems*, Inst. of Electrical and Electronics Engineers, Piscataway, NJ, 2008, pp. 280–284.

[17] Orr, J., and Shtessel, Y., "Robust Control of Lunar Spacecraft Powered Descent Using a Second Order Sliding Mode Technique," AIAA Paper 2008-6815, Aug. 2008.

[18] Massey, T., and Shtessel, Y., "Satellite Formation Control Using Traditional and High Order Sliding Modes," AIAA Paper 2004-5021, Aug. 2004.

[19] Tournes, C., and Shtessel, Y., "Predictive Launcher Guidance Using Second Order Sliding Mode Control," AIAA Paper 2006-6799, Aug. 2006.